ARTICLE

Troponin-I–induced tropomyosin pivoting defines thin-filament function in relaxed and active muscle

William Lehman[1] and Michael J. Rynkiewicz[1]

Regulation of the crossbridge cycle that drives muscle contraction involves a reconfiguration of the troponin–tropomyosin complex on actin filaments. By comparing atomic models of troponin–tropomyosin fitted to cryo-EM structures of inhibited and Ca^{2+}-activated thin filaments, we find that tropomyosin pivots rather than rolls or slides across actin as generally thought. We propose that pivoting can account for the Ca^{2+} activation that initiates muscle contraction and then relaxation influenced by troponin-I (TnI). Tropomyosin is well-known to occupy either of three meta-stable configurations on actin, regulating access of myosin motorheads to their actin-binding sites and thus the crossbridge cycle. At low Ca^{2+} concentrations, tropomyosin is trapped by TnI in an inhibitory B-state that sterically blocks myosin binding to actin, leading to muscle relaxation. Ca^{2+} binding to TnC draws TnI away from tropomyosin, while tropomyosin moves to a C-state location over actin. This partially relieves the steric inhibition and allows weak binding of myosin heads to actin, which then transition to strong actin-bound configurations, fully activating the thin filament. Nevertheless, the reconfiguration that accompanies the initial Ca^{2+}-sensitive B-state/C-state shift in troponin–tropomyosin on actin remains uncertain and at best is described by moderate-resolution cryo-EM reconstructions. Our recent computational studies indicate that intermolecular residue-to-residue salt-bridge linkage between actin and tropomyosin is indistinguishable in B- and C-state thin filament configurations. We show here that tropomyosin can pivot about relatively fixed points on actin to accompany B-state/C-state structural transitions. We argue that at low Ca^{2+} concentrations C-terminal TnI domains attract tropomyosin, causing it to bend and then pivot toward the TnI, thus blocking myosin binding and contraction.

Introduction

Head-to-tail-linked tropomyosin coiled coils form cables that span the length of actin-containing thin filaments in virtually all animal cells (Brown and Cohen, 2005; Hitchcock-DeGregori, 2008; Holmes and Lehman, 2008). The positioning of the tropomyosin cables across the surface of actin is not fixed, and in striated muscle fibers is defined by troponin, Ca^{2+} levels, and myosin-head interaction (Gordon et al., 2000; Holmes and Lehman, 2008; Lehman, 2016). By occupying one of three meta-stable configurations, tropomyosin is thought to influence the access of myosin motorheads to their actin-binding sites (Gordon et al., 2000; Poole et al., 2006; Geeves, 2012; Lehman, 2016). Accordingly, tropomyosin controls muscle contractility either by inhibiting or facilitating the myosin crossbridge cycle on actin. At low intracellular Ca^{2+} concentrations in resting, relaxed muscles, tropomyosin is thought to be trapped by the C-terminal domain of troponin-I (TnI) subunit of the troponin complex in an inhibitory B-state that blocks the myosin head binding to actin and therefore the initiation of the crossbridge cycle. Ca^{2+} binding to troponin-C (TnC) of the complex draws

the inhibitory C-terminal domain of TnI away from actin–tropomyosin to relocate onto the TnC N-lobe domain (Marston and Zamora, 2020; Yamada et al., 2020; Lehman et al., 2021). Thus, the reversible binding and translocation of this relatively short domain between TnC and actin–tropomyosin is a lynchpin in the muscle regulatory process (Ramos, 1999; Blumenschein et al., 2006; Galińska-Rakoczy et al., 2008; Sheng and Jin, 2016; Wong et al., 2019; Hornos et al., 2021; Tobacman and Cammarato, 2021). The change in TnI association is accompanied by an ~15 Å movement of tropomyosin to a C-state location over actin, relieving the steric inhibition and allowing weak binding of myosin heads to the now partially exposed actin-binding interface (Lehman et al., 1994; Gordon et al., 2000; Poole et al., 2006; Lehman, 2016; Risi et al., 2017; Risi et al., 2021a; Yamada et al., 2020). Unfettered by TnI, the tropomyosin cable is thought to oscillate about the C-state position on actin with patches of weakly bound myosin heads then transitioning to strongly actin-bound configurations (Maytum et al., 2008; Geeves, 2012). In turn, myosin binding causes a further

[1]Department of Pharmacology, Physiology and Biophysics, Boston University Chobanian and Avedisian School of Medicine, Boston, MA, USA.

Correspondence to William Lehman: wlehman@bu.edu.

tropomyosin movement another ~25 Å away from the B-state to an M-state position. The open M-state configuration of tropomyosin then facilitates the binding of neighboring myosin heads, thereby fully activating the thin filament (Vibert et al., 1997; Behrmann et al., 2012; Lehman, 2016). This stepwise forward and reverse process is integral to the "Three-State Steric Model" that has been proposed to explain the on–off switching mechanism governing all striated muscles (McKillop and Geeves, 1993; Geeves, 2012; Lehman, 2017). At the same time, crossbridge cycling on thin filaments is additionally influenced by varying myosin head recruitment from thick filaments, possibly modulated by phosphorylation, strain, or the direct effects of Ca^{2+} (Lehman, 1978; Linari et al., 2015; Fusi et al., 2016; Kampourakis et al., 2016; Craig and Padrón, 2022; Ma et al., 2022). In this article, we concentrate on Ca^{2+}-sensitive gating of myosin binding sites on actin by troponin–tropomyosin.

Despite the attractive simplicity of the steric model's description of thin filament regulation, the exact structural changes that are integral to the Ca^{2+}-sensitive B-state/C-state shifts in troponin and tropomyosin on actin remain uncertain. For example, precise delineation of B- and C-state tropomyosin positions on actin are difficult to define at atomic resolution because corresponding interactions between thin filament components are dynamic and occur over a huge structural scale (discussed in Rynkiewicz et al., 2022). At best, the transitions between tropomyosin, troponin, and actin are revealed as static moderate-resolution cryo-EM end-points (Yamada et al., 2020; Risi et al., 2021a). In contrast, the solution of the larger myosin-induced movement of the tropomyosin to the M-state position on actin appears to be less problematic (Doran et al., 2020; Doran et al., 2023a; Baldo et al., 2021). In this case, the reconfiguration is captured as distinct and well-defined M-state end-points (Milligan et al., 1990; Vibert et al., 1997; Poole et al., 2006; Behrmann et al., 2012; Doran et al., 2020; Doran et al., 2023a; Doran et al., 2023b; Risi et al., 2021b).

Tropomyosin is ideally adapted to interact end-to-end and continuously along actin filaments (Hitchcock-DeGregori, 2008; Holmes and Lehman, 2008; Orzechowski et al., 2014). The N- and C-terminal ends of coiled-coil tropomyosin are specialized to form short four-helix bundles with each other (Greenfield et al., 2006; Frey et al., 2010; Orzechowski et al., 2014). The resulting head-to-tail overlapping interactions thereby produce unbroken, longitudinally oriented tropomyosin cables traversing thin filaments. Moreover, tropomyosin is a modular molecule and each of its seven pseudorepeats interacts sequentially with a neighboring actin subunit that sits along the thin filament actin helix (McLachlan and Stewart, 1976; Brown and Cohen, 2005; Li et al., 2011; Orzechowski et al., 2014). However, as mentioned, the azimuthal position of the tropomyosin cables is not fixed. Indeed, the alternative azimuthal positional states assumed by the cable and spanning the length of the filament are thought to be governed by clustered electrostatic interactions between actin subunits and tropomyosin pseudorepeats (Brown and Cohen, 2005; Holmes and Lehman, 2008; Li et al., 2011; Pavadai et al., 2020a; Pavadai et al., 2020b), including residues Lys 326 and Lys 328 on actin subunits and glutamates and aspartates on each tropomyosin pseudorepeat (Brown et al., 2005;

Table 1. **Salt bridges formed between Tpm and actin residue 328 in C- and B-state thin filaments**

Tropomyosin residues making salt bridges to K328 on successive actin subunits along thin filaments	Tropomyosin pseudorepeat # and chain ID	Actin–tropomyosin inter-residue distance (Å)	
		C-state	B-state
Tpm-D20	1A	4.7	2.3
Tpm-E23	1A	2.3	6.2
Tpm-D58	2A′	4.1	2.1
Tpm-E96	3A	2.7	4.7
Tpm-D100	3A	3.9	5.0
Tpm-E138	4A′	2.6	2.6
Tpm-E177	5A	4.8	3.3
Tpm-E180	5A	3.9	5.3
Tpm-D219	6A′	3.3	3.7
Tpm-E257	7A	3.1	2.0

The extent of salt-bridge formation between tropomyosin and actin was assessed by examining potential interactions in atomic models of B-state (PDB ID 7UTL) and C-state (PDB ID 7UTI) thin filaments. Intermolecular links between tropomyosin and actin K328 occur on all actin subunits and involve common tropomyosin residue contacts in both B- and C-states. Tip-to-tip distances between NH_3^+ hydrogen atoms on lysine 328 of successive actin subunits along filaments and COO^- oxygen atoms of aspartate and glutamate residues on neighboring tropomyosin (Tpm) pseudorepeats were measured in UCSF Chimera (Petterson et al., 2004) and are listed for those closely apposed residues common to both states. The linkage between tropomyosin and actin residue K326 that is maintained in both B- and C-states also occurs but is more sporadic (e.g., involving tropomyosin residues E23 and E222, data not shown) and matches those previously reported (Pavadai et al., 2020a; Pavadai et al., 2020b; also see Risi et al., 2022). Numerous linkages that are either B- or C-state specific, but not common to both models augment the interactions observed (see Fig. S2). Note that because tropomyosin is a modular two-chained helical coiled-coil, its component A and A′ chain α-helices alternate with each other to form salt bridges on the successive actin subunits along thin filaments. As designated by Brown and Cohen (2005), tropomyosin pseudorepeats 1–7 are numbered to encompass tropomyosin residues 1–46, 47–85, 86–125, 126–164, 165–204, and 205–243, 244–284.

Li et al., 2011; Pavadai et al., 2020a; Pavadai et al., 2020b; Rynkiewicz et al., 2022). These positional states are separated from each other by low-energy barriers and thus are likely to easily alternate amongst themselves unless influenced further by troponin or myosin (Lehman et al., 2000; Pirani et al., 2005; Li et al., 2011; Risi et al., 2021a).

The relative alignment of actin and tropomyosin pseudorepeats and the azimuthal locations of the tropomyosin coiled-coil on thin filaments indicate that intermolecular residue-to-residue salt bridge formation between the two proteins is much the same in B- and C-state thin filament configurations (Pavadai et al., 2020a; Pavadai et al., 2020b; Rynkiewicz et al., 2022; Table 1). Considering this equivalence, how then is it possible for tropomyosin to reposition, let alone slide or roll over actin between

B- and C-states, as has been variously proposed (McLachlan and Stewart, 1976; Holthauzen et al., 2004; Li et al., 2010; Behrmann et al., 2012; von der Ecken et al., 2015; Risi et al., 2017; Lehman et al., 2020)? We suggest here that neither sliding nor rolling motions describe B- to C-state tropomyosin transitions accurately; instead, we propose that central domains of tropomyosin molecules pivot back and forth about relatively fixed points near their head-to-tail junctions, and that this pivoting accounts for the apparent B- to C-state positional shift. In effect, pivoting changes the average center-of-mass of the tropomyosin on actin and thus the azimuthal position of tropomyosin's superhelical axis in B- and C-states but does not alter the binding site linkages between tropomyosin and actin. We argue that at resting low-Ca^{2+} concentration, C-terminal domains of TnI attract the edge of the tropomyosin coiled-coil which then bends toward TnI. This motion produces the B-state filament configuration without disrupting contact between tropomyosin and canonical actin binding sites. We expect that muscle activation and ensuing C-terminal TnI detachment from actin–tropomyosin involves tropomyosin pivoting back to its C-state orientation. Our view is supported by new computational studies that complement existing cryo-EM reconstructions.

Materials and methods
Atomic models matched to cryo-EM volumes
B- and C-state atomic models of the human cardiac thin filament (PDB IDs 7UTL and 7UTI, respectively) were taken from Rynkiewicz et al. (2022) and used as reference starting structures for analysis. To date, these models most accurately and precisely fit to actin and tropomyosin contained in cryo-EM reconstructions of thin filament preserved under low- and high-Ca^{2+} conditions (Yamada et al., 2020; Risi et al., 2022; see Fig. S1). Generation of these models involved molecular dynamics flexible fitting routines (MDFF; Trabuco et al., 2009) and extensive energy minimization (Liebschner et al., 2019) of atomic models of tropomyosin, the troponin core-domain, TnT1, and the C-terminal TnI when bound to actin–tropomyosin and fitted to the cryo-EM structures (as described in Rynkiewicz et al. [2022] and below). The resulting 7UTI and 7UTL atomic models are representations only of structures that are resolved in the cryo-EM reconstructions as noted by Yamada et al. (2020) and Risi et al. (2021a).

MD simulation of 7UTI and 7UTL models
Since the 7UTI and 7UTL models do not contain full 284-residue tropomyosin chains, the tropomyosin was built out and the model extended to include 28 actin subunits, 8 tropomyosin coiled coils, and 4 troponin complexes in a periodic system, which was then used for MD simulations performed in an explicit solvent in the presence of 150 mM NaCl and 3 mM MgCl$_2$. The periodic boundary system was chosen to simulate what in essence is an infinitely long filament. First, the PDB structures were translated to the origin and aligned along the z-axis. Next, a copy of the structure was moved up to extend the filament by aligning actin chain B onto chain P (7UTL) or chain D onto chain R (7UTI). For the periodic boundary, the helical rotation of the

actin must be 167.1° rather than the 166.5° observed in the PDB structure. To relieve any strain on the filament caused by forcing the filament into the periodic system, starting outside the tropomyosin head-to-tail overlap junction and proceeding in each direction along the filament sequentially by pseudorepeat, the actins with their associated tropomyosin/troponin chains were rotated 1°. This results in the outer pseudorepeats being rotated a total of 6°. At this point, the tropomyosin chains from each copy were joined together at the closest backbone positions to create final full-length tropomyosin chains consisting of residues 1–36 of chains W and Z and residues 37–284 of chains a and b or residues 1–72 of chains g and h and residues 73–284 of chains i and j for 7UTL. For 7UTI, the full tropomyosin consisted of residues 1–42 of chains W and b and residues 43–284 of chains e and f or residues 1–53 of chains g and h and residues 54–284 of chains i and j. The full-length chains were then minimized locally using α-helical constraints obtained by running the program Coot (Emsley et al., 2010) at residues 34–39, 70–75, 40–45, 51–57, 61–66, 103–108, 140–145, 185–190, and 221–226 to fix any poor bonds created by the above manipulations of the structure.

This full tropomyosin and the associated actin and troponin chains were then copied using the actin helical symmetry to create the full filament. Before adding solvent molecules, an additional four actin subunits, as well as tropomyosin and troponin T1 chains were added to the ends of the model to serve as placeholders for the periodic boundary. Solvent atoms were then added using the solvate plugin in the graphics program VMD (Humphrey et al., 1996) with a final box size of 200 Å × 200 Å × 766.196 Å for 7UTL and 200 Å × 200 Å × 764.718 Å for 7UTI. After the removal of the placeholder chains, the system was neutralized and salt concentrations were adjusted to 0.15 M NaCl and 3 mM MgCl$_2$ using the ionize plugin in VMD (Humphrey et al., 1996). Before the simulation, the system was minimized in the CHARMM36m force field (Huang et al., 2017) and a non-bonded cutoff of 14 Å with switching using NAMD version 2.13 tools (Phillips et al., 2005; Phillips et al., 2020) in two steps. First, the solvent molecules were minimized and then the whole system was minimized with a slow release of harmonic constraints to the starting coordinates. Next, the system was heated to 300 K at constant volume with constraints to the minimized coordinates followed by a slow release of the constraints at constant temperature and volume. At this point, the pressure in the system was brought up to about 1 bar using the Nosé-Hoover Langevin piston, which was maintained through the remainder of the simulation. The simulation was then allowed to proceed without constraints. For analysis, each of the four copies of tropomyosin/troponin in each model was treated as an independent replica.

MD simulation of thin filament segments containing C-terminal TnI and tropomyosin pseudorepeats 3–5
MD was also run on a short three-actin long thin filament model containing the 7UTL B-state configuration of the C-terminal domain of TnI (residues 155–210) on actin, but here superposed on its cognate, the three-actin long C-state actin–tropomyosin structure. The corresponding three pseudorepeat long tropomyosin included residues 90–192, thus the truncated tropomyosin lacked its head-to-tail overlap and interactions

with TnT1. To prevent the ends of the tropomyosin helices from unwinding during the simulation, the backbone φ and ψ angles of the first three residues and the backbone O–NH n,n+4 hydrogen bond distances over the first five residues were constrained to known α-helical values. To prevent the tropomyosin segment from dissociating from actin during MD, a harmonic distance constraint was imposed to maintain side chains between actin residues K326 and K328 and eight of the closest neighboring glutamates on tropomyosin within a 0.8 Å standard deviation distribution of their 3.9 Å average tip-to-tip distances. This procedure kept tropomyosin at 37.1 ± 0.8 Å radius while preventing wobble about the tropomyosin superhelix along actin. However, tropomyosin was free to move azimuthally as a unit and to bend locally; thus, movement of the tropomyosin toward TnI could be assessed. The system was minimized and MD was carried out as above in explicit solvent.

Other methods
Interaction energy calculations were performed using the NAMD Energy plugin in VMD (Humphrey et al., 1996). All calculations and simulations used the CHARMM36m force field (Huang et al., 2017). Tropomyosin's helical parameters were calculated using the program, TWISTER (Strelkov and Burkhard, 2002). Molecular graphics were carried out using UCSF-Chimera and VMD programs (Pettersen et al., 2004; Humphrey et al., 1996).

Online supplemental material
Fig. S1 illustrates the fitting of C-state and B-state atomic models of the human cardiac thin filament to matching high- and low-Ca^{2+} filament reconstructions. Fig. S2 compares the interaction energetics between residues of actin and tropomyosin along the above B-state and C-state atomic models as well as the corresponding energetics during MD simulations carried out on these models. Videos 1 and 2 show the movement of C-state tropomyosin toward TnI during MD.

Results
Approach
As mentioned, steric regulation of muscle contraction involves a sequential process in which thin filaments are activated in at least two steps. Thin filaments first transition from a blocked, low-Ca^{2+} B-state characteristic of relaxed muscles to an intermediate Ca^{2+}-induced C-state and then to a final myosin-induced M-state characteristic of actively contracting muscle. We previously examined the final myosin-induced, M-state tropomyosin transitions on actin at atomic level resolution (Kiani et al, 2019; Doran et al, 2020, 2023a; Doran and Lehman, 2021). In the current analysis, we dissect the initial Ca^{2+}-dependent tropomyosin transition by comparing the organization of low-Ca^{2+} B-state and high-Ca^{2+} C-state thin filaments at near-atomic resolution. Our objective is to better define how TnI mediates tropomyosin's steric interference of myosin binding sites on actin in resting muscle and then how such steric hindrance is reversed in contracting muscle. Ever-improved atomic models defined by cryo-EM reconstructions of cardiac thin filaments

now provide an opportunity to determine tropomyosin organization, interactions, energetics, and dynamics on actin in low- and high-Ca^{2+} states (Yamada et al., 2020; Pavadai et al., 2020a; Pavadai et al., 2020b; Risi et al., 2021a; Rynkiewicz et al., 2022). By examining tropomyosin configurations with a precision previously lacking, we can disambiguate prior confusion about tropomyosin rolling or sliding between B- and C-regulatory states on actin. As we report, tropomyosin appears to do neither, rather it reconfigures locally by TnI-induced pivoting.

Tropomyosin asymmetries
When viewed from the surface of each actin subunit, tropomyosin coiled coils display seven broad and narrow motifs that reflect the twisting of their two-chained coiled-coil helices (Fig. 1, A and B). This face-on appearance replicates that of the wide and tapered tropomyosin densities seen in surface views of F-actin–tropomyosin reconstructions (see Fig. S1). Each of the seven modular tropomyosin pseudorepeats is associated with a neighboring actin subunit along the thin filament, suggesting perfect symmetry. However, individual pseudorepeats are not identical copies of each other (Brown et al., 2005; Hitchcock-DeGregori, 2008; Li et al., 2010; Pavadai et al., 2020a; Pavadai et al., 2020b; hence the term pseudorepeat). Thus, the potential regional steric effects on myosin binding may vary from one actin subunit to the next. Moreover, the tropomyosin coiled coil is thought to behave as a dynamic semiflexible rod (Li et al., 2010) creating additional positional uncertainty. Any deviation from strict superhelical symmetry no doubt is also influenced by tropomyosin form-fitting to its actin substrate. For example, idealized axial projection of B- and C-state tropomyosin superhelices along actin may not account for subtle pseudorepeat nonuniformity or capture additional azimuthal variance associated with the effects of troponin on tropomyosin tracks along actin (Fig. 1). It is very likely that current comparison of B- and C-state actin–tropomyosin conformation provides only partial cues needed to characterize the roles of tropomyosin and troponin in the steric regulatory mechanism (Tobacman, 2021; Rynkiewicz et al, 2022). To fully elucidate this regulatory process, we suggest that the local and aggregate variance in tropomyosin position along with actin and the corresponding effect of TnI on B-state tropomyosin must be rigorously and systematically evaluated. We find that this can be best achieved by comparison of recent atomic-resolution B- and C-state filament models as described below.

Mapping tropomyosin in the thin filament models
Atomic models of B- and C-state filaments (PDB IDs 7UTI and 7UTL) were generated to accurately fit to the Yamada et al. (2020) cryo-EM reconstructions of cardiac thin filaments preserved under low- and high-Ca^{2+} conditions (EMDB 0728 and 0729, respectively; Fig. 1, A and B). These refined PDB coordinates (Rynkiewicz et al, 2022) were chosen over those previously reported by Yamada et al. (2020) and subsequently employed by Risi et al. (2022; PDB IDs 6KN7 and 6KN8) since the longitudinal alignment of tropomyosin on actin was incorrectly calibrated in the earlier reports (see Pavadai et al, 2020a, 2020b; Baldo et al, 2021; Rynkiewicz et al, 2022). The revised 7UTI and
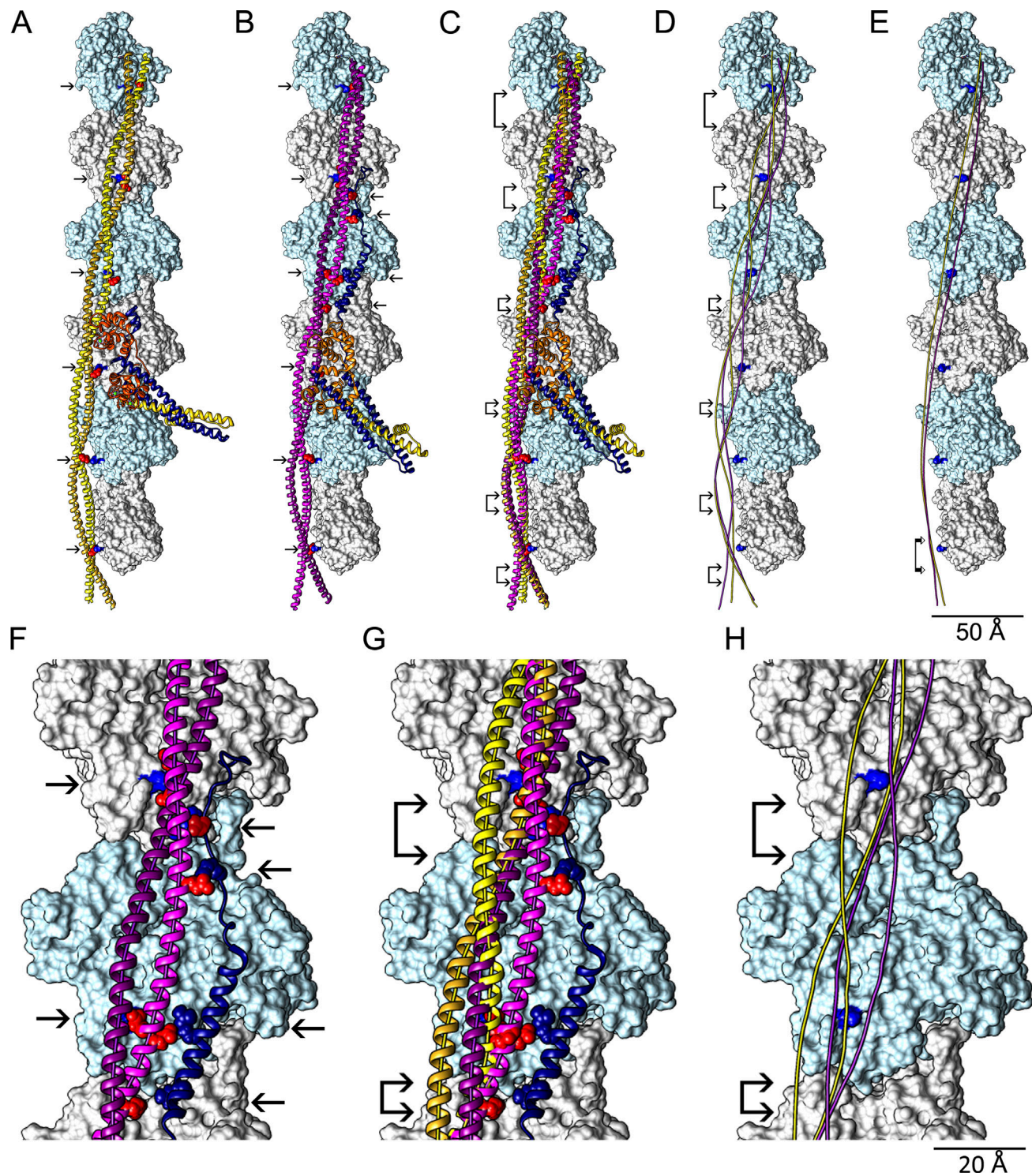
Figure 1. **Thin filament C- and B-state structures drawn from PDB** 7UTI **and** 7UTL **coordinates. (A)** The C-state, high-Ca^{2+} filament. **(B)** The B-state, low-Ca^{2+} filament. **(C)** The high and low-Ca^{2+} filaments superposed. All panels display the solvent-excluded surface of actin subunits rendered to only show the front-facing strand of actin for clarity (actin subunits colored light blue, light grey). The pointed ends of actin are shown facing up. Troponin and tropomyosin are presented in ribbon format in A–C. Color scheme: TnI, navy blue; TnC, orange; TnT, yellow; tropomyosin in its high-Ca^{2+} position, gold; and at low-Ca^{2+}, magenta. The troponin core domain, where TnI, TnC, and TnT converge, points toward the barbed end of the filament. Note: Left-facing arrows point to the navy blue TnI C-terminal domain extension on the outer actin domains in B; also note the apparent movement of the magenta low-Ca^{2+} tropomyosin strand toward TnI. **(A–C)** Salt bridges between Lys 328 on actin (blue spheres) and acidic residues on tropomyosin (red spheres) are highlighted in A and B by right-handed arrows; again note that a residue on inner tropomyosin α-helices contact K328 of each actin subunit shown (canonical salt-bridge contacts listed in Table 1; other actin–tropomyosin contacts are provided in Fig. S2). The TnI C-terminal domain, which is released from TnC at low-Ca^{2+}, is seen to bind to tropomyosin by means of salt bridges (indicated by left-handed arrows in B as well as by red and navy blue spheres in B and C). Non-polar interactions of TnI with tropomyosin and actin are not highlighted here but are discussed in Lehman et al. (2021). **(D)** The two-component α-helical tracks of coiled-coil

tropomyosin that are defined by the high- and low-Ca²⁺ tropomyosin trajectories in C are rendered as gold and magenta threads and superposed on actin. In C and D, sites marked by arrowed brackets show regions where one set of α-helical chains of the superposed high- and low-Ca²⁺ tropomyosin coiled coils coincide within a 2-Å cutoff, while the rest diverge. This is most easily seen in D by noting the overlaying threads. This positional commonality extends over contiguous tropomyosin residues 65–74, 103–109, 148–151, 188–192, 233–244, and 262–269, located in pseudorepeats 2–7; the tropomyosin head-to-tail junction is not depicted here, but is detailed in Pavadai et al. (2020a); Pavadai et al. (2020b); and Risi et al. (2022). **(E)** The superhelical tracts defined by high- and low-Ca²⁺ tropomyosin are rendered here as gold and magenta threads, respectively, and represent the average center of mass of low- and high-Ca²⁺ tropomyosin on actin (magenta and gold, respectively); note the distance between the magenta and gold threads, which are furthest apart over middle actin subunits shown, i.e., between tropomyosin pseudorepeats 3–5, and they are closest together between C-terminal tropomyosin residues 248 and 265 (indicated by broad arrowed brackets at the bottom of the panel). Actin residues 328 are highlighted as blue spheres in D and E for reference. **(F–H)** Magnified versions of B–D focused on regions in which the C-terminal domain of TnI interacts with actin and tropomyosin.

7UTL coordinates and corresponding refined tropomyosin:actin geometry define residue-to-residue contacts most relevant to elucidating the mode of tropomyosin motions between B- and C-state configurations; they do not include hypothesized representations of unresolved densities in the EM maps.

Comparison of the updated B- and C-state models clearly confirms the well-recognized difference in the azimuthal positioning of tropomyosin on actin (Fig. 1, C and D), as originally reported (Lehman et al., 1994; Vibert et al., 1997; Poole et al., 2006; Yamada et al., 2020; Risi et al., 2021a). The difference is greatest between the two tropomyosin cables over pseudorepeats 3–5 (cf. Yamada et al., 2020; Pavadai et al., 2020a; Pavadai et al., 2020b). Here, B-state pseudorepeats approach the extended form of the C-terminal domain of TnI that is released from TnC at low Ca²⁺ levels and runs roughly parallel to tropomyosin, as described by Yamada et al. (2020) and Lehman et al. (2021). Thus, tropomyosin seemingly is drawn toward the TnI domain producing the well-recognized regional azimuthal shift (Fig. 1 C; and Fig. 2, C–G).

Superposition of the new models shows that the superhelical paths formed by B- and C-state tropomyosin are separated by ∼9 to 16 Å midway along the above-described region of the tropomyosin molecule (Fig. 1 E). When side chains are included in the calculations, the outer edge of B-state tropomyosin and the inner edge of C-state tropomyosin are separated by up to 30 Å. However, our calculations show that the distinction between B- and C-state tropomyosin paths is below 2.4 Å between residues 248 and 265 (Fig. 1 E). This proximity occurs close to the C-terminal end of tropomyosin as the chains approach the head-to-tail domain. It is in this region that tropomyosin colocalizes and binds strongly to helical domains of TnT (Pavadai et al., 2020a; Pavadai et al., 2020b; Risi et al., 2022), possibly serving to pin both B- and C-state tropomyosin chains on actin at a common site.

Tropomyosin pivoting
As described above, the superposition of the B- and C-state models clearly shows the component tropomyosin strands running in parallel as they wrap around the actin filament helix. Both B- and C-regulatory state maps show that both use the same set of 10 acidic residues distributed along tropomyosin to bind to actin. These residues interact closely with Lys 328 present on each successive actin subunit of the thin filaments (Fig. 1, A and B). The salt-bridge interactions formed between tropomyosin and actin are documented in Table 1 and Fig. S2).

Transverse sections of the superposed models further illustrate periodic interactions between tropomyosin and actin as well as confirm the distinct and varying B- and C-state configurations assumed by tropomyosin on actin (Figs. 2 and 3). When sectioning through the superposed maps, a conspicuous and complementary pattern of tropomyosin B/C-state profiles repeats itself roughly every 40 residues, i.e., occurs once for every tropomyosin pseudorepeat. The pattern is most obvious at points of superposition close to the above-mentioned actin and TnI binding sites where one of the two α-helical chains from the B-state tropomyosin and one of the two helices from the C-state coiled coil overlap and appear as concentric rings in the superposed sections (Fig. 2, C–G; and Fig. 3, A–F). In marked contrast to such juxtaposition, the other non-overlapping pair of chains diverge and orient themselves in opposite directions away from the well-matched pair (Figs. 2 and 3). Here, the latter B-state tropomyosin chain is angled toward the outer domain of actin, while the C-state chain is oriented toward the inner domain of actin (Figs. 2 and 3) as if the tropomyosin coiled-coil bends in the B-state by forming attractive electrostatic linkages and hydrophobic interactions with TnI (best visualized in Fig. 2, C–G). Not surprisingly, the magnitude of the bending of the B-state tropomyosin coiled-coil away from the C-state copy is greatest for tropomyosin residues contained in pseudorepeats 3 to 5 that lie next to the TnI C-terminal extension on B-state filaments (Figs. 1, 2, and 3). It therefore is likely that the B-state to C-state reorientation is caused locally by C-terminal TnI attachment and detachment to and from tropomyosin, as previously concluded (Yamada et al., 2020). Indeed, the bending appears to diminish toward pseudorepeats adjacent to the tropomyosin head-to-tail intermolecular junction, and, for example, is minimal over pseudorepeat seven as tropomyosin converges on the tropomyosin overlapping domain (Fig. 1), namely, where, as mentioned above, tropomyosin may also interact strongly with the TnT1 tail domain of TnT (Pavadai et al., 2020a; Pavadai et al., 2020b; Risi et al., 2022). With tropomyosin repositioning minimal near its head-to-tail overlap domain and greatest over more central domains (pseudorepeats 3–5), it follows that the B/C-state tropomyosin reconfiguration does not represent a global rolling or sliding motion of tropomyosin coiled-coil cables over actin but rather a pivoting between relatively fixed ends. Bear in mind that the tropomyosin pseudorepeat contact points on successive actin residues mentioned above to Lys 328 (Fig. 1, A–C; and Table 1) are unchanged in the B- and C-regulatory states. The observation is consistent with the view that these contacts are pivot point fulcrums for the tropomyosin motion (Table 1), as docking studies on actin–tropomyosin segments originally suggested (Pavadai et al., 2020a; Pavadai et al., 2020b; Doran et al., 2020).
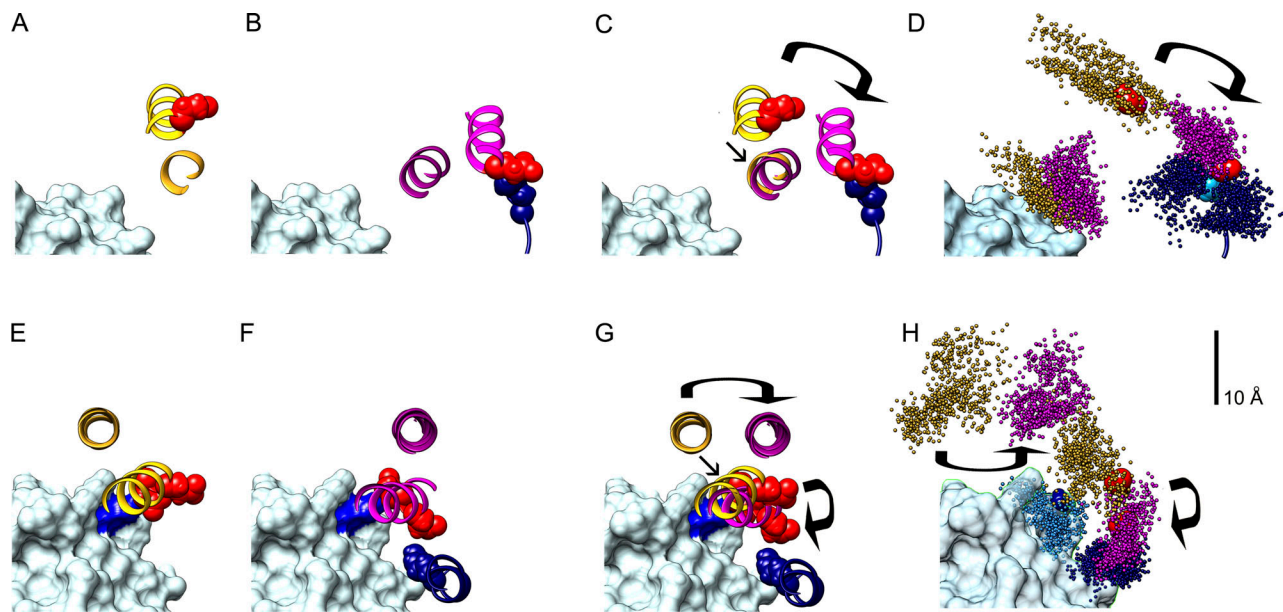
Figure 2. **TnI-induced pivoting of tropomyosin.** Transverse sections of C- and B-state thin filament structures shown in Fig. 1 viewed here over C-terminal TnI residues R192 (A–C) and R170 (E–G); these TnI residues localize in close proximity to tropomyosin E114 and E139. (A and E) C-state sections (B and F), B-state sections, (C and G), B- and C-state sections superposed (same color representation as in Fig. 1). **(D and H)** Corresponding dynamics of tropomyosin and TnI shown in superposed sections. **(A–C)** Sections highlight tropomyosin pivoting, and in B and C salt-bridge formation between tropomyosin E114 (red spheres) and TnI residue R192 (navy blue spheres). Note that in C, superposition of B- and C-state sections shows inner tropomyosin helices overlapping (short arrow), while TnI appears to have drawn the outer tropomyosin helix toward the B-state position (bold arrow). **(E–G)** Sections highlight tropomyosin pivoting and salt-bridge formation of tropomyosin E138 with actin residue K328 (blue on actin surface), and in F and G, a salt bridge between tropomyosin E139 with TnI residue R170 (navy blue spheres). Note that in G, the superposition of B- and C-state sections shows inner tropomyosin helices are closely apposed (short arrow), while TnI appears to attract tropomyosin E139 of the inner tropomyosin helix (oblique bold arrow) here, causing the outer helix to pivot toward the B-state position (horizontal bold arrow). **(D and H)** Representation of tropomyosin and TnI dynamics on actin observed during MD simulations viewed in sections in D corresponding to ones in A and B and in H to E and F. The data are from the last 12 ns of simulations and represent 109 frames of B-state and 77 frames of C-state structures superposed. **(D)** Representative positions of the charged side-chain atoms of tropomyosin residue E114 (magenta and gold points for low- and high-Ca^{2+} data, respectively) and TnI residue R192 (navy blue points) taken during MD simulations of B- and C-state thin filament models (magenta and gold points show the positions of negatively charged Glu OE1 and OE2 atoms on E114, respectively, and navy blue points for positively charged Arg atoms NH1, NH2, and NE on R192). **(H)** Analogously rendered positions of negatively charged side-chain atoms on tropomyosin residue E139 and positively charged atoms on TnI residue R170 during MD simulations again performed on B- and C-state filaments (same color scheme as above); points assumed by positively charged NZ atoms actin residue K328 in H also shown for reference (light blue). The red and cyan spheres in D and H show the respective COO$^-$ and NH$_3^+$ side-chain positions of tropomyosin and TnI at the beginning of the MD simulations; the blue sphere in Fig. 2 H shows the initial location of the terminal K328 NH$_3^+$ at the onset of MD. The curved arrows indicate the direction of tropomyosin movement toward the actin outer domain (myosin steric-blocking position) associated with tropomyosin–TnI complex formation as in C and G.

Energetics of B- and C-state thin-filament interactions

We previously described an array of polar interactions between TnI and tropomyosin (Lehman et al., 2021) and now conclude that they likely facilitate tropomyosin's pivoting between B- and C-state orientations. Indeed, measurement of thin-filament interaction energy that includes C-terminal TnI polar residues Gln 156, Arg 162, Arg 170, Lys 174, Glu 182, Arg 186, Arg 192, Asp 196, and Ser 199 increases the total interaction energy of tropomyosin and actin/troponin in B-state thin filaments and thereby favors the C-state to B-state transition (Table 2). In addition, non-polar contacts involving the TnI switch-peptide and the H$_4$ helix also likely enhance B-state linkage with tropomyosin. In
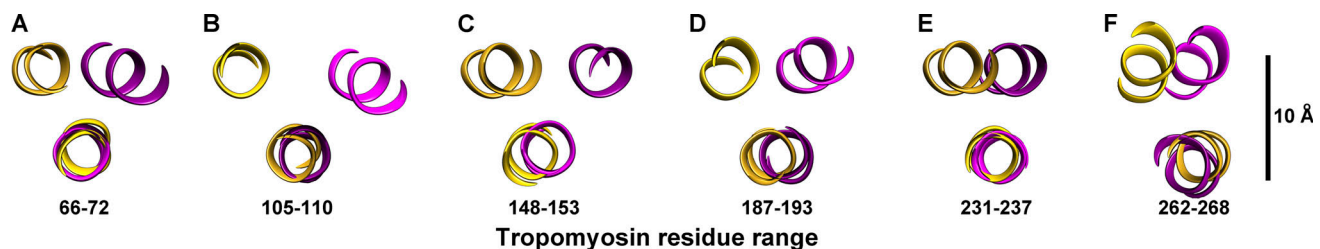

Figure 3. **C-state to B-state pivoting of tropomyosin.** Transverse sections through superposed 7UTI C-state and 7UTL B-state thin filament models but only with the tropomyosin positions displayed for comparison (gold, C-state tropomyosin; magenta, B-state tropomyosin). Selected slab sections show where the inner B- and C-state α-helices coincide, while the complementary outer pairs splay apart. This pattern is shown over tropomyosin residues 66–72, 105–110, 148–153, 187–193, 231–237, and 262–268, as indicated.

Table 2. **Interaction energy and salt bridge formation between actin, tropomyosin (Tpm), and the C-terminal domain of TnI**

	Interaction energies (kcal/mol)		Intermolecular salt bridges
	Coulombic	van der Waals	n residues involved
C-state			
Actin–Tpm pseudorepeat 2	−50	−23	1
Actin—Tpm pseudorepeat 3	−414	9	2
Actin—Tpm pseudorepeat 4	−481	−18	5
Actin—Tpm pseudorepeat 5	−242	−16	4
Actin—Tpm pseudorepeat 6	−545	−14	6
Actin—C-terminal TnI	—	—	—
Tpm—C-terminal TnI	—	—	—
Total	−1,732	−62	18
B-state			
Actin–Tpm pseudorepeat 2	−154	4	3
Actin—Tpm pseudorepeat 3	−248	−26	2
Actin—Tpm pseudorepeat 4	−285	−8	1
Actin—Tpm pseudorepeat 5	−328	−13	4
Actin—Tpm pseudorepeat 6	−498	−1	4
Actin—C-terminal TnI	−65	−95	7
Tpm—C-terminal TnI	−348	−54	12
Total	−1,926	−193	33

Electrostatic and van der Waals interactions between different thin filament pseudorepeat segments defined by B-state (PDB ID 7UTL) and C-state (PDB ID 7UTI) atomic models were measured in VMD (Humphrey et al., 1996). Salt bridges attributed to the above segments were also counted using tip-to-tip inter-residue cutoff of 5.5 Å. Values were tabulated for tropomyosin pseudorepeats 2–6 neighboring TnI. Data reported for C-terminal TnI interactions were acquired for TnI residues 149 to 210, which includes the switch-peptide, H_4 helix, and C-terminal domain of TnI (as defined by Marston and Zamora, 2020).

total these interactions, no doubt, are responsible for the B-state-directed tropomyosin pivoting initiated over tropomyosin pseudorepeats 3–5. Conversely, the energetic cost of pivoting tropomyosin toward the B-state position when the C-terminal TnI is sequestered by TnC at high Ca^{2+} concentration would diminish tropomyosin movement from its default C-state position.

MD simulations of B- and C-state thin filaments
In order to further evaluate tropomyosin organization and its motions on actin, MD simulations were performed on the 7UTI and 7UTL atomic models of C- and B-state thin filaments

containing tropomyosin, the troponin core domain, TnT, and the C-terminal domain of TnI in the latter model. Tropomyosin was noted to oscillate locally about its two starting positions while maintaining its ∼37 Å radius and the canonical salt bridge pivot points between B/C-state helices along all actin subunits described above for the duration of the 120 ns MD simulation (Fig. 2, D–H; and Fig. S2). The stability of these interactions supports our contention that tropomyosin pivoting is a native process and not a cryo-EM artifact. We also noted that during MD simulations, side-chains of C-state tropomyosin Glu 114 and 139 appear to face and sample surrounding solvent, while in the B-state motions of E114 and E139 side-chains facing TnI are more limited due to contact with C-terminal TnI domain residues R192 and R170 (Fig. 2, D–H), supporting our notion that salt-bridge linkage, at least in part, drives complex formation between TnI and tropomyosin. In this regard, the interaction between tropomyosin and the C-terminal domain of TnI, for example via Arg 192, was also shown by NMR performed on thin-filament peptides (Wong et al., 2019; Hornos et al., 2021).

Examination of Fig. 2, D–H, suggests that during MD, a fraction of the side-chains extending from C-state tropomyosin residues 114 or 139 visit the region occupied by the B-state C-terminal TnI peptide as if primed to interact at the onset of relaxation (highlighted by a slanted arrow in Fig. 2, D–H). The size of the periodic boundary system used to mimic an infinitely long thin filament (∼3 million atoms) precluded capturing the global movement of C-state tropomyosin to its B-state position during MD. To visualize the potential for such a transition, we carried out MD simulations on a reduced size C/B-state chimera containing actin and tropomyosin pseudorepeats 3–5 in their C-state positions, as well as C-terminal residues 155–210 of TnI in its B-state position; thus, TnI was placed in a position set to draw C-state tropomyosin to its B-state position. The anticipated pivoting motion of tropomyosin occurred within 10–40 ns of the onset of MD, during which salt bridges formed between residues E114 and R192 as well as between E139 and R170 (Videos 1 and 2). The simulation suggests that tropomyosin can pivot as a global unit in the direction of the C-terminal domain of TnI. However, a full description of the interaction would require understanding the docking of C-terminal TnI to actin–tropomyosin once released from the N-lobe of TnC under low-Ca^{2+} muscle relaxing conditions. In this regard, several questions remain unanswered. For example, do the components of the TnI domain, namely its switch peptide, H_4-helix, and unstructured tail-end bind to actin and tropomyosin sequentially, and in what order?

Discussion
X-ray fiber diffraction of intact tissue has previously been used to estimate the azimuthal shift of tropomyosin undergoing the B/C-state transition (Poole et al., 2006). The ∼23 Å (i.e., 15°) azimuthal movement that was calculated is considerably larger than has been observed by cryo-EM and validated here. However, contributions from the C-terminal extension of TnI (Yamada et al., 2020; Risi et al., 2021a) may not have been adequately delineated from those of tropomyosin in the fiber diffraction analysis. Thus, the inclusion of TnI contributions may

have overstated the actual amount of tropomyosin translation. Similarly, unaccounted TnI contributions as well as the effects of sample flattening may also have exaggerated the amount of B/C-state tropomyosin relocation detected in reconstructions of negatively stained filaments (Lehman et al., 1994; Vibert et al., 1997; Pirani et al., 2005).

Our observations raise obvious questions about the origin and functional significance of the seemingly small B/C-state transitions, which we now can answer. The previously proposed, rather large 15° shift in tropomyosin position between low- and high-Ca²⁺ B- and C-state positions on actin provided a heuristic understanding of troponin–tropomyosin–based steric regulation of muscle contractility. However, we now posit that steric regulation primarily involves trapping the tropomyosin coiled-coil very close to the C-state over myosin binding sites on actin. As mentioned, the effect is brought about by interactions of tropomyosin with the C-terminal domain of TnI, and the resulting B/C-state pivoting is a manifestation of this. Such pivoting does not require or involve large-scale B/C-state translation of tropomyosin over the actin surface. TnI-induced pivoting does accentuate the magnitude of myosin binding site obstruction by drawing tropomyosin over the target site, but the action of TnI clasping onto tropomyosin and trapping the coiled-coil in an inhibitory state may be what is crucial.

It has long been known that tropomyosin can inhibit acto-myosin ATPase in vitro (Lehrer and Morris, 1982, 1984) and by itself partially obstructs myosin binding sites on actin in the absence of troponin (Vibert et al., 1997; Lehman et al., 2000; Poole et al., 2006). However, troponin-free tropomyosin as well as C-state tropomyosin is thought to oscillate on actin (Pirani et al., 2005; Maytum et al., 2008). Thus, tropomyosin acting alone would be ineffective as an on–off switching mechanism, potentially allowing limited access for weakly binding myosin heads to thin filaments in B- or C-state configurations. This view is supported by observations made in vitro showing that the inhibitory effect of tropomyosin dissipates as myosin concentration is increased, enabling significant numbers of myosin heads to bind to actin–tropomyosin and transition to the M-state (Lehrer and Morris, 1982; Lehrer and Morris, 1984). Hence, TnI in the troponin-regulated thin filament is needed to augment tropomyosin-linked effects by stabilizing steric interference and preventing tropomyosin azimuthal drift. The combined troponin–tropomyosin action thus produces robust actomyosin inhibition and activation. Here, TnI is the choreographer directing the pivoting performed during the tropomyosin pirouette. Pivoting over a common set of residues is particularly advantageous for the B/C-state transition as it sidesteps the energetic cost involved in switching protein–protein interactions that tropomyosin sliding or rolling over actin would otherwise entail.

Changes observed in muscle fiber diffraction patterns 50 yr ago demonstrated tropomyosin's regulatory movement over thin filament actin (Huxley, 1972; Haselgrove, 1972; Vibert et al., 1972; Parry and Squire, 1973). These seminal studies presaged the work reported here and no doubt are consistent with the troponin–tropomyosin regulatory mechanism that we propose.

Data availability

The data underlying Figs. 1, 2, and 3; Tables 1 and 2; and Fig. S1 and Fig. S2 are derived directly from PDB coordinates 7UTI and 7UTL deposited in the RCSB Protein Data Bank (https://www.rcsb.org/). Fig. S1 can be reproduced from the same PDB files and from coordinates deposited for cryo-EM volumes (EMDB IDs 0729, 0728, 22965, and 22964) in the Electron Microscopy Data Bank (https://www.ebi.ac.uk/emdb/) using the Fit-in-Map tool in the UCSF-Chimera suite of programs (Petterson et al., 2004).

References

Baldo, A.P., J.C. Tardiff, and S.D. Schwartz. 2021. A proposed mechanism for the initial myosin binding event on the cardiac thin filament: A meta-dynamics study. *J. Phys. Chem. Lett.* 12:3509–3513. https://doi.org/10.1021/acs.jpclett.1c00223

Behrmann, E., M. Müller, P.A. Penczek, H.G. Mannherz, D.J. Manstein, and S. Raunser. 2012. Structure of the rigor actin-tropomyosin-myosin complex. *Cell.* 150:327–338. https://doi.org/10.1016/j.cell.2012.05.037

Blumenschein, T.M.A., D.B. Stone, R.J. Fletterick, R.A. Mendelson, and B.D. Sykes. 2006. Dynamics of the C-terminal region of TnI in the troponin complex in solution. *Biophys. J.* 90:2436–2444. https://doi.org/10.1529/biophysj.105.076216

Brown, J.H., and C. Cohen. 2005. Regulation of muscle contraction by tropomyosin and troponin: How structure illuminates function. *Adv. Protein Chem.* 71:121–159. https://doi.org/10.1016/S0065-3233(04)71004-9

Brown, J.H., Z. Zhou, L. Reshetnikova, H. Robinson, R.D. Yammani, L.S. Tobacman, and C. Cohen. 2005. Structure of the mid-region of tropomyosin: Bending and binding sites for actin. *Proc. Natl. Acad. Sci. USA.* 102:18878–18883. https://doi.org/10.1073/pnas.0509269102

Craig, R., and R. Padrón. 2022. Structural basis of the super- and hyper-relaxed states of myosin II. *J. Gen. Physiol.* 154:e202113012. https://doi.org/10.1085/jgp.202113012

Doran, M.H., and W. Lehman. 2021. The central role of the F-actin surface in myosin force generation. *Biology.* 10:1221. https://doi.org/10.3390/biology10121221

Doran, M.H., E. Pavadai, M.J. Rynkiewicz, J. Walklate, E. Bullitt, J.R. Moore, M. Regnier, M.A. Geeves, and W. Lehman. 2020. Cryo-EM and molecular docking shows myosin loop 4 contacts actin and tropomyosin on thin filaments. *Biophys. J.* 119:821–830. https://doi.org/10.1016/j.bpj.2020.07.006

Doran, M.H., M.J. Rynkiewicz, E. Pavadai, S.M.L. Bodt, D. Rasicci, J.R. Moore, C.M. Yengo, E. Bullitt, and W. Lehman. 2023a. Myosin loop-4 is critical for optimal tropomyosin repositioning on actin during muscle activation

and relaxation. *J. Gen. Physiol.* 155:e202213274. https://doi.org/10.1085/jgp.202213274

Doran, M.H., M.J. Rynkiewicz, D. Rasicci, S.M.L. Bodt, M.E. Barry, E. Bullitt, C.M. Yengo, J.R. Moore, and W. Lehman. 2023b. Conformational changes linked to ADP release from human cardiac myosin bound to actin-tropomyosin. *J. Gen. Physiol.* 155:e202213267. https://doi.org/10.1085/jgp.202213267

Emsley, P., B. Lohkamp, W.G. Scott, and K. Cowtan. 2010. Features and development of Coot. *Acta Crystallogr. D Biol. Crystallogr.* 66:486–501. https://doi.org/10.1107/S0907444910007493

Frye, J., V.A. Klenchin, and I. Rayment. 2010. Structure of the tropomyosin overlap complex from chicken smooth muscle: Insight into the diversity of N-terminal recognition. *Biochemistry*. 49:4908–4920. https://doi.org/10.1021/bi100349a

Fusi, L., E. Brunello, Z. Yan, and M. Irving. 2016. Thick filament mechanosensing is a calcium-independent regulatory mechanism in skeletal muscle. *Nat. Commun.* 7:13281. https://doi.org/10.1038/ncomms13281

Galińska-Rakoczy, A., P. Engel, C. Xu, H. Jung, R. Craig, L.S. Tobacman, and W. Lehman. 2008. Structural basis for the regulation of muscle contraction by troponin and tropomyosin. *J. Mol. Biol.* 379:929–935. https://doi.org/10.1016/j.jmb.2008.04.062

Geeves, M.A. 2012. Thin filament regulation. *In*: Comprehensive Biophysics, Vol. 4, E. H.Egelman, Y. E. Goldman, E. M. Ostap, editors. Oxford: Academic Press. Oxford, England. 251–267. https://doi.org/10.1016/B978-0-12-374920-8.00416-1

Gordon, A.M., E. Homsher, and M. Regnier. 2000. Regulation of contraction in striated muscle. *Physiol. Rev.* 80:853–924. https://doi.org/10.1152/physrev.2000.80.2.853

Greenfield, N.J., Y.J. Huang, G.V. Swapna, A. Bhattacharya, B. Rapp, A. Singh, G.T. Montelione, and S.E. Hitchcock-DeGregori. 2006. Solution NMR structure of the junction between tropomyosin molecules: Implications for actin binding and regulation. *J. Mol. Biol.* 364:80–96. https://doi.org/10.1016/j.jmb.2006.08.033

Haselgrove, J.C. 1972. X-ray evidence for a conformational change in the actin-containing filaments of vertebrate striated muscle. *Cold Spring Harb. Symp. Quant. Biol.* 37:341–352. https://doi.org/10.1101/SQB.1973.037.01.044

Hitchcock-DeGregori, S.E. 2008. Tropomyosin: Function follows structure. *Adv. Exp. Med. Biol.* 644:60–72. https://doi.org/10.1007/978-0-387-85766-4_5

Holmes, K.C., and W. Lehman. 2008. Gestalt-binding of tropomyosin to actin filaments. *J. Muscle Res. Cell Motil.* 29:213–219. https://doi.org/10.1007/s10974-008-9157-6

Holthauzen, L.M., F. Corrêa, and C.S. Farah. 2004. Ca²⁺-induced rolling of tropomyosin in muscle thin filaments: The α- and β-band hypothesis revisited. *J. Biol. Chem.* 279:15204–15213. https://doi.org/10.1074/jbc.M308904200

Hornos, F., H.Z. Feng, B. Rizzuti, M. Palomino-Schätzlein, D. Wieczorek, J.L. Neira, and J.-P. Jin. 2021. The muscle-relaxing C-terminal peptide from troponin I populates a nascent helix, facilitating binding to tropomyosin with a potent therapeutic effect. *J. Biol. Chem.* 296:100228. https://doi.org/10.1074/jbc.RA120.016012

Huang, J., S. Rauscher, G. Nawrocki, T. Ran, M. Feig, B.L. de Groot, H. Grubmüller, and A.D. MacKerell Jr. 2017. CHARMM36m: An improved force field for folded and intrinsically disordered proteins. *Nat. Methods*. 14:71–73. https://doi.org/10.1038/nmeth.4067

Humphrey, W., A. Dalke, and K. Schulten. 1996. VMD: Visual molecular dynamics. *J. Mol. Graph.* 14:33–38: 27–28. https://doi.org/10.1016/0263-7855(96)00018-5

Huxley, H.E. 1972. Structural changes in actin and myosin-containing filaments during contraction. Cold Spring Habor Symp. *Quant. Biol.* 37: 361–376. https://doi.org/10.1101/SQB.1973.037.01.046

Kampourakis, T., Y.-B. Sun, and M. Irving. 2016. Myosin light chain phosphorylation enhances contraction of heart muscle via structural changes in both thick and thin filaments. *Proc. Natl. Acad. Sci. USA*. 113: E3039–E3047. https://doi.org/10.1073/pnas.1602776113

Kiani, F.A., W. Lehman, S. Fischer, and M.J. Rynkiewicz. 2019. Spontaneous transitions of actin-bound tropomyosin toward blocked and closed states. *J. Gen. Physiol.* 151:4–8. https://doi.org/10.1085/jgp.201812188

Lehman, W. 1978. Thick-filament-linked calcium regulation in vertebrate striated muscle. *Nature*. 274:80–81. https://doi.org/10.1038/274080a0

Lehman, W. 2016. Thin filament structure and the steric blocking model. *Compr. Physiol.* 63:1043–1069. https://doi.org/10.1002/cphy.c150030

Lehman, W. 2017. Switching muscles on and off in steps: The McKillop-Geeves three-state model of muscle regulation. *Biophys. J.* 112: 2459–2466. https://doi.org/10.1016/j.bpj.2017.04.053

Lehman, W., R. Craig, and P. Vibert. 1994. Ca²⁺-induced tropomyosin movement in Limulus thin filaments revealed by three-dimensional reconstruction. *Nature*. 368:65–67. https://doi.org/10.1038/368065a0

Lehman, W., V. Hatch, V. Korman, M. Rosol, L. Thomas, R. Maytum, M.A. Geeves, J.E. Van Eyk, L.S. Tobacman, and R. Craig. 2000. Tropomyosin and actin isoforms modulate the localization of tropomyosin strands on actin filaments. *J. Mol. Biol.* 302:593–606. https://doi.org/10.1006/jmbi.2000.4080

Lehman, W., M.J. Rynkiewicz, and J.R. Moore. 2020. A new twist on tropomyosin binding to actin filaments: Perspectives on thin filament function, assembly and biomechanics. *J. Muscle Res. Cell Motil.* 41:23–38. https://doi.org/10.1007/s10974-019-09501-5

Lehman, W., E. Pavadai, and M.J. Rynkiewicz. 2021. C-terminal troponin-I residues trap tropomyosin in the muscle thin filament blocked-state. *Biochem. Biophys. Res. Commun.* 551:27–32. https://doi.org/10.1016/j.bbrc.2021.03.010

Lehrer, S.S., and E.P. Morris. 1982. Dual effects of tropomyosin and troponin-tropomyosin on actomyosin subfragment 1 ATPase. *J. Biol. Chem.* 257: 8073–8080. https://doi.org/10.1016/S0021-9258(18)34298-4

Lehrer, S.S., and E.P. Morris. 1984. Comparison of the effects of smooth and skeletal tropomyosin on skeletal actomyosin subfragment 1 ATPase. *J. Biol. Chem.* 259:2070–2072. https://doi.org/10.1016/S0021-9258(17)43316-3

Li, X.E., K.C. Holmes, W. Lehman, H. Jung, and S. Fischer. 2010. The shape and flexibility of tropomyosin coiled coils: Implications for actin filament assembly and regulation. *J. Mol. Biol.* 395:327–339. https://doi.org/10.1016/j.jmb.2009.10.060

Li, X.E., L.S. Tobacman, J.Y. Mun, R. Craig, S. Fischer, and W. Lehman. 2011. Tropomyosin position on F-actin revealed by EM reconstruction and computational chemistry. *Biophys. J.* 100:1005–1013. https://doi.org/10.1016/j.bpj.2010.12.3697

Liebschner, D., P.V. Afonine, M.L. Baker, G. Bunkóczi, V.B. Chen, T.I. Croll, B. Hintze, L.W. Hung, S. Jain, A.J. McCoy, et al. 2019. Macromolecular structure determination using X-rays, neutrons and electrons: Recent developments in Phenix. *Acta Crystallogr. D Struct. Biol.* 75:861–877. https://doi.org/10.1107/S2059798319011471

Linari, M., E. Brunello, M. Reconditi, L. Fusi, M. Caremani, T. Narayanan, G. Piazzesi, V. Lombardi, and M. Irving. 2015. Force generation by skeletal muscle is controlled by mechanosensing in myosin filaments. *Nature*. 528:276–279. https://doi.org/10.1038/nature15727

Ma, W., S. Nag, H. Gong, L. Qi, and T.C. Irving. 2022. Cardiac myosin filaments are directly regulated by calcium. *J. Gen. Physiol.* 154:e202213213. https://doi.org/10.1085/jgp.202213213

Maytum, R., V. Hatch, M. Konrad, W. Lehman, and M.A. Geeves. 2008. Ultra short yeast tropomyosins show novel myosin regulation. *J. Biol. Chem.* 283:1902–1910. https://doi.org/10.1074/jbc.M708593200

Marston, S., and J.E. Zamora. 2020. Troponin structure and function: A view of recent progress. *J. Muscle Res. Cell Motil.* 41:71–89. https://doi.org/10.1007/s10974-019-09513-1

McKillop, D.F.A., and M.A. Geeves. 1993. Regulation of the interaction between actin and myosin subfragment 1: Evidence for three states of the thin filament. *Biophys. J.* 65:693–701. https://doi.org/10.1016/S0006-3495(93)81110-X

McLachlan, A.D., and M. Stewart. 1976. The 14-fold periodicity in α-tropomyosin and the interaction with actin. *J. Mol. Biol.* 103: 271–298. https://doi.org/10.1016/0022-2836(76)90313-2

Milligan, R.A., M. Whittaker, and D. Safer. 1990. Molecular structure of F-actin and location of surface binding sites. *Nature*. 348:217–221. https://doi.org/10.1038/348217a0

Orzechowski, M., X.E. Li, S. Fischer, and W. Lehman. 2014. An atomic model of the tropomyosin cable on F-actin. *Biophys. J.* 107:694–699. https://doi.org/10.1016/j.bpj.2014.06.034

Parry, D.A.D., and J.M. Squire. 1973. Structural role of tropomyosin in muscle regulation: Analysis of the x-ray diffraction patterns from relaxed and contracting muscles. *J. Mol. Biol.* 75:33–55. https://doi.org/10.1016/0022-2836(73)90527-5

Pavadai, E., M.J. Rynkiewicz, A. Ghosh, and W. Lehman. 2020a. Docking troponin T onto the tropomyosin overlapping domain of thin filaments. *Biophys. J.* 118:325–336. https://doi.org/10.1016/j.bpj.2019.11.3393

Pavadai, E., W. Lehman, and M.J. Rynkiewicz. 2020b. Protein-protein docking reveals dynamic interactions of tropomyosin on actin filaments. *Biophys. J.* 119:75–86. https://doi.org/10.1016/j.bpj.2020.05.017

Pettersen, E.F., T.D. Goddard, C.C. Huang, G.S. Couch, D.M. Greenblatt, E.C. Meng, and T.E. Ferrin. 2004. UCSF Chimera—A visualization system for exploratory research and analysis. *J. Comput. Chem.* 25:1605–1612. https://doi.org/10.1002/jcc.20084

Phillips, J.C., R. Braun, W. Wang, J. Gumbart, E. Tajkhorshid, E. Villa, C. Chipot, R.D. Skeel, L. Kalé, and K. Schulten. 2005. Scalable molecular dynamics with NAMD. *J. Comput. Chem.* 26:1781–1802. https://doi.org/10.1002/jcc.20289

Phillips, J.C., D.J. Hardy, J.D.C. Maia, J.E. Stone, J.V. Ribeiro, R.C. Bernardi, R. Buch, G. Fiorin, J. Hénin, W. Jiang, et al. 2020. Scalable molecular dynamics on CPU and GPU architectures with NAMD. *J. Chem. Phys.* 153: 044130. https://doi.org/10.1063/5.0014475

Pirani, A., C. Xu, V. Hatch, R. Craig, L.S. Tobacman, and W. Lehman. 2005. Single particle analysis of relaxed and activated muscle thin filaments. *J. Mol. Biol.* 346:761–772. https://doi.org/10.1016/j.jmb.2004.12.013

Poole, K.J.V., M. Lorenz, G. Evans, G. Rosenbaum, A. Pirani, R. Craig, L.S. Tobacman, W. Lehman, and K.C. Holmes. 2006. A comparison of muscle thin filament models obtained from electron microscopy reconstructions and low-angle X-ray fibre diagrams from non-overlap muscle. *J. Struct. Biol.* 155:273–284. https://doi.org/10.1016/j.jsb.2006.02.020

Ramos, C.H. 1999. Mapping subdomains in the C-terminal region of troponin I involved in its binding to troponin C and to thin filament. *J. Biol. Chem.* 274:18189–18195. https://doi.org/10.1074/jbc.274.26.18189

Risi, C., J. Eisner, B. Belknap, D.H. Heeley, H.D. White, G.F. Schröder, and V.E. Galkin. 2017. Ca^{2+}-induced movement of tropomyosin on native cardiac thin filaments revealed by cryoelectron microscopy. *Proc. Natl. Acad. Sci. USA.* 114:6782–6787. https://doi.org/10.1073/pnas.1700868114

Risi, C.M., I. Pepper, B. Belknap, M. Landim-Vieira, H.D. White, K. Dryden, J.R. Pinto, P.B. Chase, and V.E. Galkin. 2021a. The structure of the native cardiac thin filament at systolic Ca^{2+} levels. *Proc. Natl. Acad. Sci. USA.* 118:e2024288118. https://doi.org/10.1073/pnas.2024288118

Risi, C., L.U. Schäfer, B. Belknap, I. Pepper, H.D. White, G.F. Schröder, and V.E. Galkin. 2021b. High-resolution cryo-EM Structure of the cardiac actomyosin complex. *Structure.* 29:50–60.e4. https://doi.org/10.1016/j.str.2020.09.013

Risi, C.M., B. Belknap, H.D. White, K. Dryden, J.R. Pinto, P.B. Chase, and V.E. Galkin. 2022. High-resolution cryo-EM structure of the junction region of the native cardiac thin filament in relaxed state. *PNAS Nexus.* 2: pgac298. https://doi.org/10.1093/pnasnexus/pgac298

Rynkiewicz, M.J., E. Pavadai, and W. Lehman. 2022. Modeling human cardiac thin filaments. *Front. Physiol.* 13:932333. https://doi.org/10.3389/fphys.2022.932333

Sheng, J.J., and J.-P. Jin. 2016. TNNI1, TNNI2 and TNNI3: Evolution, regulation, and protein structure-function relationships. *Gene.* 576:385–394. https://doi.org/10.1016/j.gene.2015.10.052

Strelkov, S.V., and P. Burkhard. 2002. Analysis of α-helical coiled coils with the program TWISTER reveals a structural mechanism for stutter compensation. *J. Struct. Biol.* 137:54–64. https://doi.org/10.1006/jsbi.2002.4454

Tobacman, L.S. 2021. Troponin revealed: Uncovering the structure of the thin filament on-off switch in striated muscle. *Biophys. J.* 120:1–9. https://doi.org/10.1016/j.bpj.2020.11.014

Tobacman, L.S., and A. Cammarato. 2021. Cardiomyopathic troponin mutations predominantly occur at its interface with actin and tropomyosin. *J. Gen. Physiol.* 153:e202012815. https://doi.org/10.1085/jgp.202012815

Trabuco, L.G.E., E. Villa, E. Schreiner, C.B. Harrison, and K. Schulten. 2009. Molecular dynamics flexible fitting: A practical guide to combine cryo-electron microscopy and X-ray crystallography. *Methods.* 49:174–180. https://doi.org/10.1016/j.ymeth.2009.04.005

Vibert, P., R. Craig, and W. Lehman. 1997. Steric-model for activation of muscle thin filaments. *J. Mol. Biol.* 266:8–14. https://doi.org/10.1006/jmbi.1996.0800

Vibert, P.J., J.C. Haselgrove, J. Lowy, and F.R. Poulsen. 1972. Structural changes in actin-containing filaments of muscle. *Nat. New Biol.* 236: 182–183. https://doi.org/10.1038/newbio236182a0

von der Ecken, J., M. Müller, W. Lehman, D.J. Manstein, P.A. Penczek, and S. Raunser. 2015. Structure of the F-actin-tropomyosin complex. *Nature.* 519:114–117. https://doi.org/10.1038/nature14033

Wong, S., H.Z. Feng, and J.-P. Jin. 2019. The evolutionarily conserved C-terminal peptide of troponin I is an independently configured regulatory structure to function as a myofilament Ca^{2+}-desensitizer. *J. Mol. Cell. Cardiol.* 136:42–52. https://doi.org/10.1016/j.yjmcc.2019.09.002

Yamada, Y., K. Namba, and T. Fujii. 2020. Cardiac muscle thin filament structures reveal calcium regulatory mechanism. *Nat. Commun.* 11:153. https://doi.org/10.1038/s41467-019-14008-1
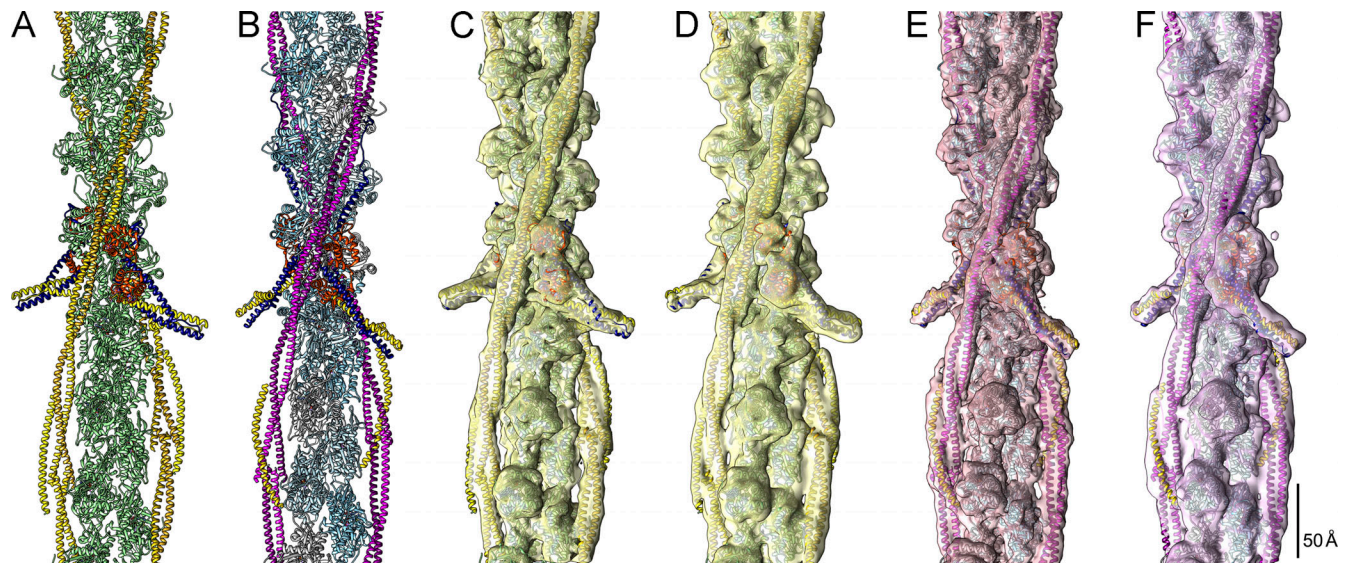
Figure S1.   **Fitting atomic models of cardiac thin filaments to cryo-EM reconstructions. (A and B)** Atomic models of the high-Ca^{2+} C-state (A; PDB ID 7UTI) and the low-Ca^{2+} B-state (B; PDB ID 7UTL) thin filaments. The pointed ends of actin are shown facing up. Actin, tropomyosin, and troponin are presented in ribbon format (actin subunits in A are in green and in B are blue; tropomyosin chains in A are in gold and in B are magenta; TnI, navy blue; TnC, orange; TnT, yellow). **(C–F)** The C-state atomic model in A was fitted to the high-Ca^{2+} cardiac thin filament reconstructions generated by Yamada et al. (2020) in C (EMDB ID 0729) and by (Risi et al, 2021a) in D (EMDB ID 22965), while B-state atomic model in B was fitted to reconstructions of low-Ca^{2+} filaments produced by Yamada et al. (2020) in E (EMDB ID 0728) and by (Risi et al, 2021a) in F (EMDB ID 22964). Please note the excellent fitting of the atomic models to corresponding reconstructions. Also note that the individual helices forming the tropomyosin strand in E are better defined than in F, which was consistent with a marginally higher cross-correlation of the atomic model in B to the reconstruction volume in E.

Electrostatic interactions of tropomyosin to actin residues K326/K328

A Comparison of B-state (7UTL) and C-state (7UTI) models
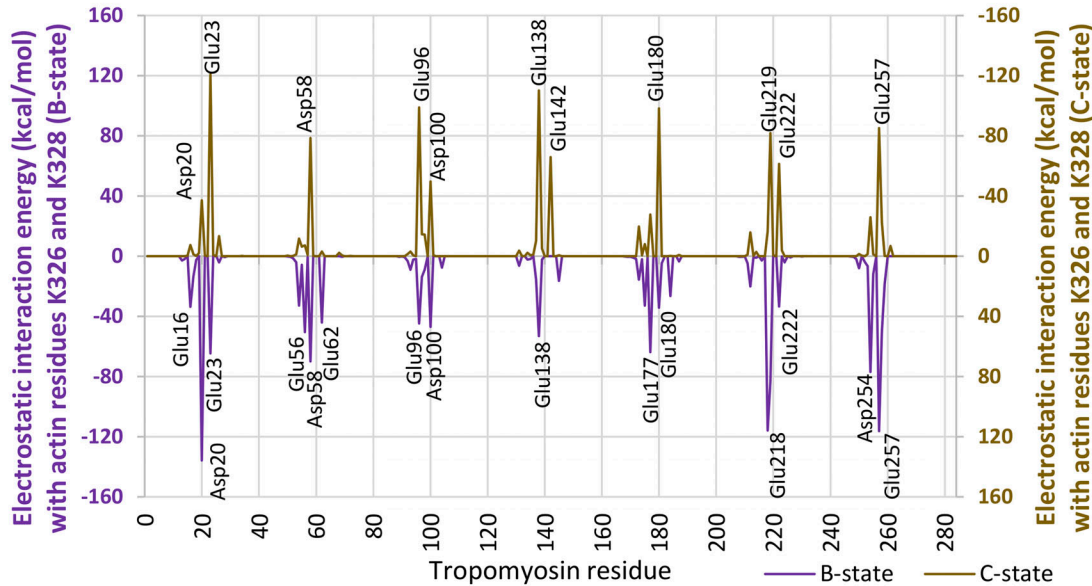
B Comparison of B-state (7UTL) and C-state (7UTI) models during MD
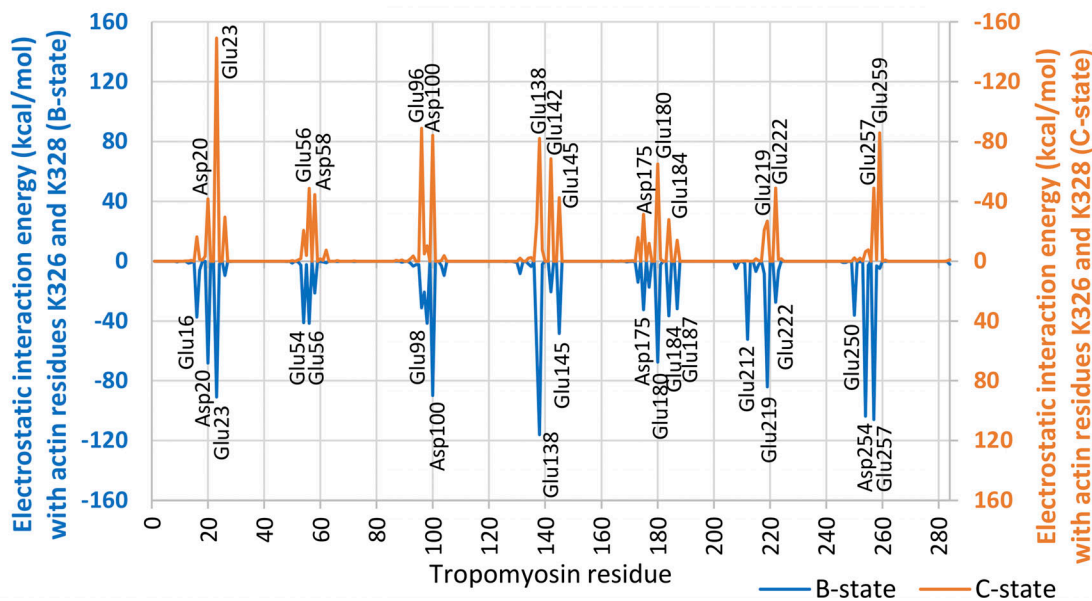

Figure S2. **Measurement of electrostatic interaction between actin and tropomyosin along thin filaments. (A and B)** Electrostatic interaction energy between individual tropomyosin residues and actin residues 326 and 328 were plotted for atomic models of C- and B-state filaments (A; PDB IDs 7UTI and 7UTL) and for data taken from MD simulations carried out on the models and then energies averaged over 120 ns of the procedure (B). The peaks observed in these plots pinpoint salt bridges between actin and tropomyosin and the magnitude of the peaks indicates the corresponding strength of the interactions. Note that the same set of closely neighboring residues are involved in salt-bridge interactions in the B- and C-state filaments, and that this pattern persists during MD. The residue pairs involved are numbered.

Video 1.   **C- to B-state transition of tropomyosin moving toward TnI residue 192.** This video highlights the region containing tropomyosin residue E114 moving toward R192 on TnI and shows MD simulation of C-state tropomyosin pivoting to the B-state position. Cross-sectional views were taken from the 44-ns simulation highlighting the C-state tropomyosin (yellow) beginning on actin as localized in the PDB 7UTI model and then transitioning to the B-state position in the presence of C-terminal domain of TnI (blue); a static model of B-state tropomyosin (magenta) is superposed for reference.

Video 2.   **C- to B-state transition of tropomyosin moving toward TnI residue 170.** This video highlights the region containing tropomyosin residue E139 moving toward R170 on TnI and shows MD simulation of C-state tropomyosin pivoting to the B-state position. Cross-sectional views were taken from the 44-ns simulation highlighting the C-state tropomyosin (yellow) beginning on actin as localized in the PDB 7UTI model and then transitioning to the B-state position in the presence of C-terminal domain of TnI (blue); a static model of B-state tropomyosin (magenta) is superposed for reference. Note the salt bridge contacts formed during MD and the tropomyosin pivoting. The respective glutamate and arginine side-chain atoms are shown as red and blue spheres. The color representation matches that in Fig. 2.